frontiers in Mechanical Engineering

ORIGINAL RESEARCH
published: 24 March 2020
doi: 10.3389/fmech.2020.00014

Proof of Concept and Preliminary Results of Gas Detection by Measuring the Admittance at the Resonance and Anti-resonance of an Uncoated CMUT

*Luis Iglesias[1], Priyadarshini Shanmugam[2], Jean-François Michaud[2], Daniel Alquier[2], Dominique Certon[2] and Isabelle Dufour[1]**

[1] Université de Bordeaux, Laboratoire IMS UMR-CNRS 5218, Talence, France, [2] Université de Tours, GREMAN UMR-CNRS 7347, Tours, France

OPEN ACCESS

Edited by:
Silvan Schmid,
Vienna University of Technology,
Austria

Reviewed by:
Qin Zhou,
University of Nebraska-Lincoln,
United States
Daniel Hernández-Cruz,
Autonomous University of Chiapas,
Mexico

***Correspondence:**
Isabelle Dufour
isabelle.dufour@ims-bordeaux.fr

Specialty section:
This article was submitted to
Micro- and Nanoelectromechanical
Systems,
a section of the journal
Frontiers in Mechanical Engineering

Received: 13 December 2019
Accepted: 03 March 2020
Published: 24 March 2020

Citation:
Iglesias L, Shanmugam P,
Michaud J-F, Alquier D, Certon D and
Dufour I (2020) Proof of Concept and
Preliminary Results of Gas Detection
by Measuring the Admittance at the
Resonance and Anti-resonance of an
Uncoated CMUT.
Front. Mech. Eng. 6:14.
doi: 10.3389/fmech.2020.00014

Functionalized films are commonly used in gas sensing to target a particular gas. This is due, in part, to their usually high capability to detect very low concentrations and their high selectivity. However, their poor stability over time remains a challenge when dealing with applications that require the sensing to remain reliable without frequent recalibration. For this reason, uncoated gas sensors have become increasingly popular regardless of their lower sensitivity and their often non-selective characteristics. There exist different approaches for gas sensing without a functionalized film. One possibility is to use an uncoated resonating sensor and tracking its resonant properties which depend on its surrounding environment. The easy integration capability of capacitive micromachined ultrasonic transducers (CMUTs) makes them great candidates for uncoated gas sensing. Moreover, they are able to reach very high resonant frequencies and, therefore, allow for a shorter response time. In this article, a method to detect gas by following the value of the admittance of an uncoated silicon nitride CMUT array at either the resonant or at the anti-resonant frequency is presented and tested. This chemical detection is purely based on the change of the physical properties of the gas mixture (the mass density and the viscosity). A general model describing the impact of the electrical and mechanical properties of the CMUT in the sensitivity is presented, validated and applied to carbon dioxide and methane detection.

Keywords: CMUT, capacitive sensor, MEMS, uncoated sensors, gas sensing, resonator

1. INTRODUCTION

In gas sensing, coating a device with a thin film specifically tailored to chemically interact with the target analyte is by far the most common approach (Göpel, 1994; Park et al., 2007; Lee et al., 2011; Qiu et al., 2015). However, it has been shown that using a sensitive coating compromises the long term stability of the sensor (Korotcenkov and Cho, 2011) mostly due to aging of such film (Sharma et al., 2001; Romain and Nicolas, 2010). For this reason, there is an increasing interest toward uncoated sensors, which rely on the change of the physical properties of their surrounding gas such as thermal conductivity (Daynes, 1933; Hale et al., 1992; Simon and Arndt, 2002), or mass

density (Tétin et al., 2010; Boudjiet et al., 2014; Rosario and Mutharasan, 2014). Despite the lack of selectivity of uncoated sensors, it is still possible to discriminate from different gases by measuring multiple parameters at once (Iglesias et al., 2019).

It has been shown that both the resonant frequency and the quality factor of uncoated resonant sensors such as microcantilever resonators depend on physical properties of the fluid surrounding them (Sader, 1998; Abdolrazzaghi and Daneshmand, 2016). This has been used previously for characterizing liquids (Heinisch et al., 2015) and even gases, despite the fact that their mass density and viscosity are much smaller. Gas detection such as hydrogen, carbon dioxide, argon, helium and methane detection have already been demonstrated using uncoated resonant sensors (Tétin et al., 2010; Boudjiet et al., 2014; Rosario and Mutharasan, 2014; Iglesias et al., 2019). These measurements have been performed either using silicon or piezoelectric cantilevers at frequencies below 200 kHz. However, capacitive micromachined ultrasonic transducers (CMUTs) (Haller and Khuri-Yakub, 1996) present an advantage over piezoelectric resonators due to their relatively easy integration (Törndahl et al., 2002; Wygant et al., 2008; Gurun et al., 2011; Um et al., 2014). Additionally, gas sensing has already been done with uncoated ultrasonic microresonators by measuring the time of flight of a signal propagating through the gas (Toda and Kobayakawa, 2008; Shanmugam et al., 2018). Nevertheless, a physical gas detection using the measurement of the admittance spectrum of an uncoated silicon nitride CMUT array has, to the best of our knowledge, never been done. The principle, which is based on the measurement of the value of the admittance at the resonance and anti-resonance and not on the corresponding frequency shifts, along with an analytical model of the impact of a change in the gas composition, are presented and verified under mixtures of nitrogen and either carbon dioxide (CO_2) or methane (CH_4) as an example.

The principle of this method along with the experimental setup and results will be presented in the following sections.

2. MATERIALS AND METHODS

2.1. Sensor and Model

Schematics of a single Capacitive Micromachined Ultrasonic Transducer (CMUT) like the one used in this study are shown in **Figure 1A**. The microfabrication process based on surface micromachining can be found in Heller et al. (2018). By applying a voltage V between the electrodes, the silicon nitride membrane deflects, changing the capacitance of the sensor.

It has been shown previously that a simple lumped model as the one in **Figure 1B** can describe accurately the behavior of a single CMUT (Wenchao et al., 2008; Koymen et al., 2017) and it results in the following equation corresponding to Newton's second law of motion:

$$m\frac{\partial^2 u}{\partial t^2} = \frac{1}{2}\frac{\epsilon_0 A V^2}{(h_{eq}-u)^2} - c\frac{\partial u}{\partial t} - ku, \tag{1}$$

where k is the stiffness of the membrane, c the linear damping coefficient (depending on the viscous losses in the gas), m the displaced mass (of both the membrane and the surrounding gas), u the displacement of the membrane, V the actuation voltage, ϵ_0 the vacuum dielectric constant, A the surface of the membrane and h_{eq} the equivalent gap of the CMUT, whose expression is:

$$h_{eq} = h_{gap} + \frac{t_m}{\epsilon_r}, \tag{2}$$

where h_{gap} is the gap between the dielectric membrane and the bottom electrode at rest ($V = 0$), t_m the thickness of the membrane and ϵ_r the relative permittivity of the membrane.

In such case, by considering that:

$$V = V_{dc} + V_{ac}, \tag{3}$$

where V_{dc} is the bias and V_{ac} the excitation voltage, it can be shown that, at a given V_{dc} such that $V_{ac} << V_{dc}$, the harmonic electrical admittance Y of a single CMUT can be expressed as:

$$Y = j\omega C_0 \frac{k}{k_s}\frac{1 + j\frac{c}{k}\omega - \frac{m}{k}\omega^2}{1 + j\frac{c}{k_s}\omega - \frac{m}{k_s}\omega^2}, \tag{4}$$

where j is such that $j^2 = -1$, ω the angular frequency of the excitation, C_0 the static electrical capacitance and k_s the stiffness of the membrane by taking into account the electrostatic softening. The expression of k_s and C_0 are:

$$k_s = k - \frac{\epsilon_0 A V_{dc}^2}{(h_{eq}-u_{dc})^3}, \tag{5}$$

$$C_0 = \frac{\epsilon_0 A}{h_{eq}-u_{dc}}, \tag{6}$$

where u_{dc} is the static displacement of the membrane corresponding to $V = V_{dc}$.

From Equation (4), under vacuum and assuming no solid viscous losses (Koymen et al., 2017) ($c = 0$), the vacuum admittance resonant ($\omega_{r,0}$) and anti-resonant ($\omega_{a,0}$) angular frequencies can be defined. Their expressions are:

$$\omega_{r,0} = \sqrt{\frac{k_s}{m}}, \tag{7}$$

$$\omega_{a,0} = \sqrt{\frac{k}{m}}. \tag{8}$$

Similarly, the corresponding quality factors ($c \neq 0$) of the admittance resonance (Q_r) and anti-resonance (Q_a) can be defined:

$$Q_r = \frac{\sqrt{k_s m}}{c}, \tag{9}$$

$$Q_a = \frac{\sqrt{km}}{c}. \tag{10}$$

The CMUT's electromechanical coupling coefficient (k_t) (Yaralioglu et al., 2003) is introduced as:

$$k_t^2 = 1 - \left(\frac{\omega_{r,0}}{\omega_{a,0}}\right)^2 = \frac{2u_{dc}}{h_{eq}-u_{dc}}, \tag{11}$$

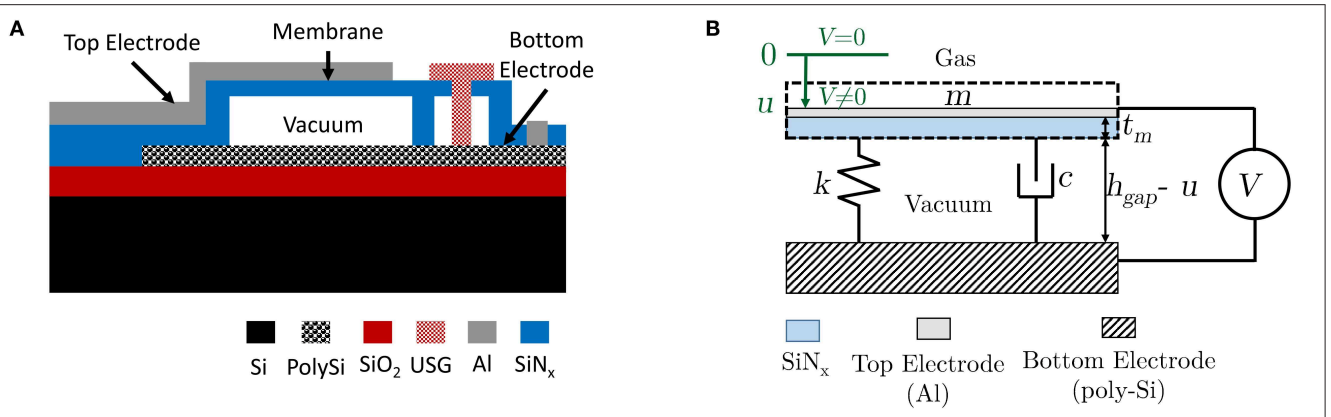

FIGURE 1 | (A) Schematic view of a single CMUT from this study where USG stands for Undoped Silicon Glass. **(B)** Lumped model schematics of a single CMUT.

Equations (6), (7), and (9) can then be rearranged:

$$C_0 = \frac{\epsilon_0 A(2+k_t^2)}{2h_{eq}}, \tag{12}$$

$$\omega_{r,0} = \omega_{a,0}\sqrt{1-k_t^2}, \tag{13}$$

$$Q_r = Q_a\sqrt{1-k_t^2}, \tag{14}$$

which leads to the final expression of Y:

$$Y = j\omega C_{00} Y_n, \tag{15}$$

where C_{00} is the capacitance without bias ($k_t = 0$):

$$C_{00} = \frac{\epsilon_0 A}{h_{eq}}, \tag{16}$$

and Y_n the normalized admittance containing all the information about the resonant properties of the CMUT. Its expression is:

$$Y_n = \frac{(2+k_t^2)}{2(1-k_t^2)} \frac{1 + j\frac{1}{Q_a}x - x^2}{1 + j\frac{1}{Q_a(1-k_t^2)}x - \frac{1}{(1-k_t^2)}x^2}, \tag{17}$$

where:

$$x = \frac{\omega}{\omega_{a,0}}. \tag{18}$$

The modulus of the reduced admittance $|Y_n|$ is maximum at $x = x_r$ and minimum at $x = x_a$:

$$x_r = \sqrt{1 - \frac{k_t^2}{2} - \frac{\sqrt{Q_a^2 k_t^4 - 2k_t^2 + 4}}{2Q_a}}, \tag{19}$$

$$x_a = \sqrt{1 - \frac{k_t^2}{2} + \frac{\sqrt{Q_a^2 k_t^4 - 2k_t^2 + 4}}{2Q_a}}. \tag{20}$$

Their corresponding values, respectively, $|Y_r|_{max}$ and $|Y_r|_{min}$, are:

$$|Y_n|_{max} = \frac{2+k_t^2}{2}\sqrt{\frac{Q_a^2 k_t^4 + 4x_r^2 + \delta(1+Q_a^2 k_t^2)}{Q_a^2 k_t^4 + 4x_r^2 + \delta(1-Q_a^2 k_t^2)}}, \tag{21}$$

$$|Y_n|_{min} = \frac{2+k_t^2}{2}\sqrt{\frac{Q_a^2 k_t^4 + 4x_a^2 - \delta(1+Q_a^2 k_t^2)}{Q_a^2 k_t^4 + 4x_a^2 - \delta(1-Q_a^2 k_t^2)}}, \tag{22}$$

where:

$$\delta = x_a^2 - x_r^2 = \frac{1}{Q_a}\sqrt{Q_a^2 k_t^4 - 2k_t^2 + 4}. \tag{23}$$

Therefore both, $|Y_n|_{max}$ and $|Y_n|_{min}$, depend only on both Q_a and k_t. From Equation (11), one could argue that, at a fixed polarization, k_t still depends on the gas through $\omega_{r,0}$ or ω_{a_0}. However, from Equation (1) in static:

$$0 = \frac{1}{2}\frac{\epsilon_0 A V_{dc}^2}{(h_{eq} - u_{dc})^2} - k u_{dc}, \tag{24}$$

u_{dc} depends only on k, ϵ_0, A, V_{dc}, and h_{eq}. None of which depend on the gas properties. This means, according to Equation (11), that at fixed polarization k_t is constant. However, a change in the gas composition induces a change dQ_a in Q_a. Therefore one can expect to see a change in $|Y_n|_{max}$ and $|Y_n|_{min}$ as well. At this point, it should be highlighted that x_r is only defined for values of k_t below a critical value k_c for which $x_r = 0$:

$$k_c = \sqrt{2 - \frac{2Q_a^2}{2Q_a^2 - 1}} \approx 1, \tag{25}$$

which happens close to the collapse voltage V_{coll}. Finally, by differentiating Equations (21) and (22), at fixed k_t, it comes:

$$\frac{d|Y_n|_{max}}{|Y_n|_{max}} = \alpha_r \frac{dQ_a}{Q_a}, \tag{26}$$

$$\frac{d|Y_n|_{min}}{|Y_n|_{min}} = \alpha_a \frac{dQ_a}{Q_a}, \tag{27}$$

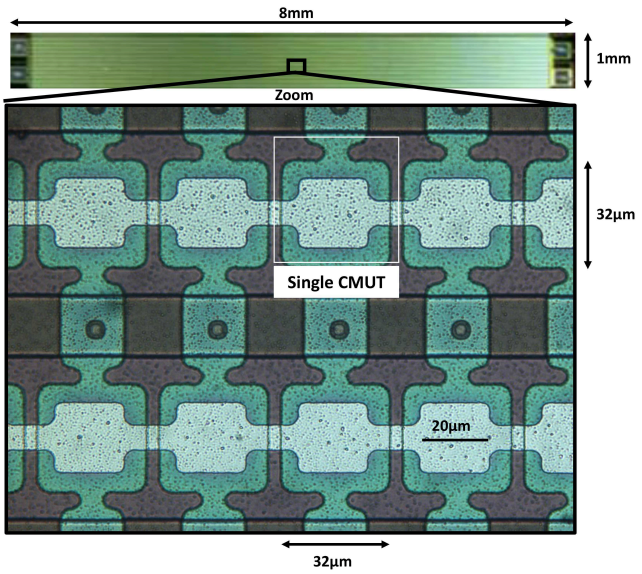

FIGURE 2 | Picture of the array (~ 8 mm × 1 mm) composed of thousands of single CMUTs in parallel and zoom. Membrane dimensions: 32 μm × 32 μm × 450 nm, $\omega_a = 50$ rad/µs, $Q_a = 33$, $V_{coll} = 58$V.

where α_r and α_a are the electrical gains in sensitivity at the resonance and anti-resonance, respectively. Their expressions are:

$$\alpha_r = \frac{-4k_t^2 x_r^2 Q_a^2}{8x_r^2 + 2Q_a^2 k_t^4 + \delta[3 + 2Q_a^2(k_t^2 - 2)]}, \quad (28)$$

$$\alpha_a = \frac{-4k_t^2 x_a^2 Q_a^2}{8x_a^2 + 2Q_a^2 k_t^4 - \delta[3 + 2Q_a^2(k_t^2 - 2)]}. \quad (29)$$

By analyzing the difference $\Delta\alpha$:

$$\Delta\alpha = |\alpha_r| - |\alpha_a| = \frac{4Qa^2 k_t^2}{(2Q_a - 1)(2Q_a + 1)[4Q_a^2(k_t^2 - 1) + 1]}, \quad (30)$$

it is possible to show that $\Delta\alpha < 0$ for $k_t^2 < 1 - 1/(4Q_a^2)$ which is the case in practice since $k_c^2 < 1 - 1/(4Q_a^2)$. Therefore, the sensitivity is always higher by tracking $|Y_n|_{min}$ instead of $|Y_n|_{max}$. That being said, for typical values of Q_a (10–1,000) and k_t^2 (below 0.3), this difference is rather small (below 1%).

It is worth noticing that the formulae of this section 2.1 are the same for an array of identical CMUTs in parallel like the one shown in **Figure 2**. Nevertheless the overall variations are added with a higher number of CMUTs, which improves the signal to noise ratio.

At this point, the model can be applied to all kinds of sensing where the principle is to track the admittance peaks of a CMUT. In the particular case of gas sensing with an uncoated CMUT array, m and c will change due to the effect of the gas (air or N_2 for instance) and will modify the quality factor Q_a. Finally, the sensitivity to a particular gas will depend both on its viscosity and its mass density through dQ_a (viscous losses).

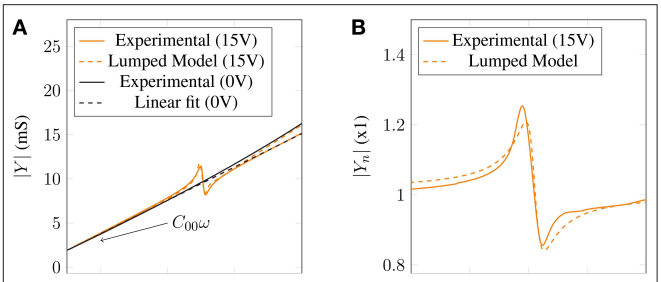

FIGURE 3 | Comparison between experimental and theoretical values under N_2 ($k_t^2 = 0.011$, $V_{dc} = 15$V, $Q_a = 33$, $\omega_{a,0} = 50$ rad/µs). **(A)** $|Y|$ as a function of ω. **(B)** $|Y_n|$ as a function of ω.

2.2. Model Validation

In order to compare the model, some parameters of the model need to be determined by the measured admittance $|Y(\omega)|$.

The parameters $\omega_{r,0}$ (in N_2) and Q_r (in N_2) were extracted from the measured conductance G, which is the real part of the admittance Y:

$$G = \omega C_0 \frac{k_t^2}{1 - k_t^2} \frac{\frac{\omega}{\omega_{r,0} Q_r}}{\left(\frac{\omega}{\omega_{r,0} Q_r}\right)^2 + \left(\frac{w^2}{w_{r,0}^2} - 1\right)^2}. \quad (31)$$

Indeed, the maximum of G, named G_{max}, is for $\omega = \omega_{r,0}$ and Q_r can be estimated by using:

$$Q_r = \frac{\omega_{r,0}}{\Delta\omega}, \quad (32)$$

where $\Delta\omega$ is the bandwidth at $G = G_{max}/2$.

C_{00} was obtained by measuring the slope of $|Y(\omega)|$ at $V_{dc} = 0$V as shown in **Figure 3A** for which the value $C_{00} = 190$pF was obtained. Knowing the value of C_{00} allowed to compute $|Y_n| = |Y|/(C_{00}\omega)$ for different values of V_{dc}. It allowed to determine the value of k_t by using Equation (33):

$$k_t^2 = \frac{2H_0 - 2}{2H_0 + 1}, \quad (33)$$

where:

$$H_0 = \lim_{x \to 0} |Y_n|(x) = \frac{2 + k_t^2}{2(1 - k_t^2)}. \quad (34)$$

Knowing $\omega_{r,0}$, Q_r and k_t, $\omega_{a,0} = 50$ rad/µs and $Q_a = 33$ are simply obtained by using Equations (13) and (14), respectively.

Figure 3B shows the experimental values of $|Y_n|$ (solid) for $V_{dc} = 15$V and its expression (Equation 17) resulting from the lumped model approximation (dashed) as a function of ω. Both curves are in agreement with each other. The mismatch can be explained by the simplicity of the model. Indeed, neither a particular geometry nor a non-uniformity between the array elements (Lee et al., 2009) have been considered. Also, in order to verify experimentally that the sensitivity at the resonance is comparable at the one at the anti-resonance, the relative

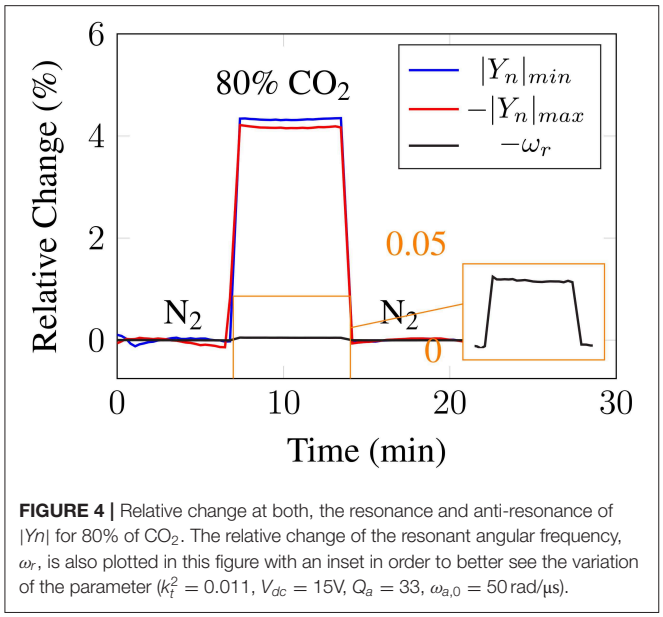

FIGURE 4 | Relative change at both, the resonance and anti-resonance of $|Yn|$ for 80% of CO_2. The relative change of the resonant angular frequency, ω_r, is also plotted in this figure with an inset in order to better see the variation of the parameter ($k_t^2 = 0.011$, $V_{dc} = 15$V, $Q_a = 33$, $\omega_{a,0} = 50$ rad/μs).

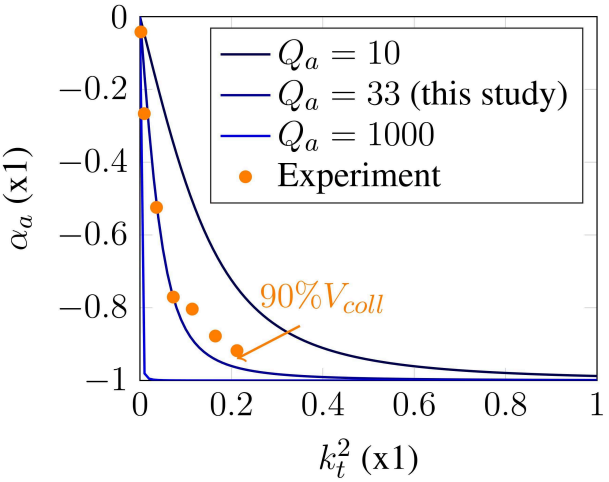

FIGURE 5 | α_a as a function of k_t. 4% of CO_2 in N_2 was used to measure $d|Y_n|_{min}/|Y_n|_{min}$ and the corresponding dQ_a.

change in admittance was measured in both cases while the gas composition was changed from pure N_2 to 80% of CO_2 in N_2. The results, shown in **Figure 4**, confirm the barely higher sensitivity in the case of the anti-resonance. Moreover, in **Figure 4**, the relative change of the resonant angular frequency, ω_r, during the same experiment has been plotted. It can be easily concluded that, with this particular device, tracking the admittance at either the resonance or anti-resonance is much more sensitive than the typical method of tracking the resonant angular frequency (gas detection step only visible in the inset of **Figure 4**).

Additionally, verification of the expression of α_a from Equation (29) is shown in **Figure 5** where the theoretical values are shown for different values of Q_a as a function of k_t (solid lines). The experimental values were obtained through Equation (27) by monitoring $|Y_n|_{min}$ for V_{dc} varying from 1V to 52V (90% of V_{coll}) in order to avoid damaging the sensors. For each value of V_{dc}, 4% of CO_2 was introduced in order to be able to measure $d|Y_n|_{min}$ even for low values of k_t. The obtained dQ_a from the obtained values of Q_a is $dQ_a = -0.126$ (for the case $V_{dc} = 35$V). These values are also plotted (orange dots) and are in agreement with the theory. The obtained values are reported in **Table 1**.

Intuitively (and this is confirmed by the plot of α_a in **Figure 5**), for gas detection, one should try to get as close to V_{coll} as possible (taking into account V_{ac}) in order to reach the highest sensitivity. However, the noise standard deviation (σ) increases as well with V_{dc} (Wygant et al., 2016) and, therefore, the limit of detection (LOD), which can be approximated by Equation (35) (Lange et al., 2002), does not necessarily improve.

$$LOD = \frac{3\sigma}{S}, \tag{35}$$

where S is the overall sensitivity to a particular gas. For this reason, the results presented in the following section were carried out at 60% of V_{coll} ($V_{dc} = 35$V) where the best trade-off between noise and sensitivity was measured.

3. RESULTS AND DISCUSSION

3.1. Changing the Gas

In order to test the performances of this method, tests where pure N_2 is alternated with either CO_2 (heavier gas) or CH_4 (lighter gas) at different concentrations (4%, 3%, 2%, 1%) were performed. The relative variation of $|Y_n|_{min}$ with respect to N_2 ($d|Y_n|_{min}/|Y_n|_{min}$) for both sequences is shown, in **Figures 6A,B**, respectively. The temperature drift was compensated by removing the slow varying background.

These results where used afterwards to plot the calibration curves (**Figure 7**) which show good linearity (at least for that concentration range). Therefore, the sensitivity of the sensor S can be defined for each mixture (N_2 and either CO_2 or CH_4) as the slope of the calibration curve. These values are $S_{CO2} = 6.9.10^{-4}$/% and $S_{CH4} = -5.3.10^{-4}$/%.

In the simpler case of a cantilever respecting Euler-Bernoulli conditions and for small variations, $d\rho$ and $d\eta$ of the mass density ρ and the viscosity η of the gas, it can be shown that the quality factor Q varies (Iglesias et al., 2019):

$$\frac{dQ}{Q} = -a\frac{d\rho}{\rho} - b\frac{d\eta}{\eta}, \tag{36}$$

where a and b are positive constants depending on the geometry and the main gas (N_2 in this case). Reported values of $d\rho/\rho$ and $d\eta/\eta$ for 1% of either CO_2 and CH_4 are presented in **Table 2**.

Therefore, since for CH_4 $d\rho$ and $d\eta$ (with respect to N_2) are both negative, the sign of S_{CH4} is consistent with the theory ($\alpha_a < 0$). Moreover, given the sign of S_{CO2} and considering that, in the case of CO_2, $d\rho > 0$ and $d\eta < 0$ this indicates that the effect of the mass density is dominant over the one of the viscosity. Indeed, by applying Equation (36) to CO_2 and CH_4 to

TABLE 1 | Experimental values used in **Figure 3**.

V_{dc} (V)	1	15	30	40	46	50	52
k_t^2 (%)	0.2	0.9	4	7	11	17	21
$d\|Y_n\|_{min}/\|Y_n\|_{min}$ (‰)	0.15	1.0	2.0	2.9	3.0	3.3	3.5

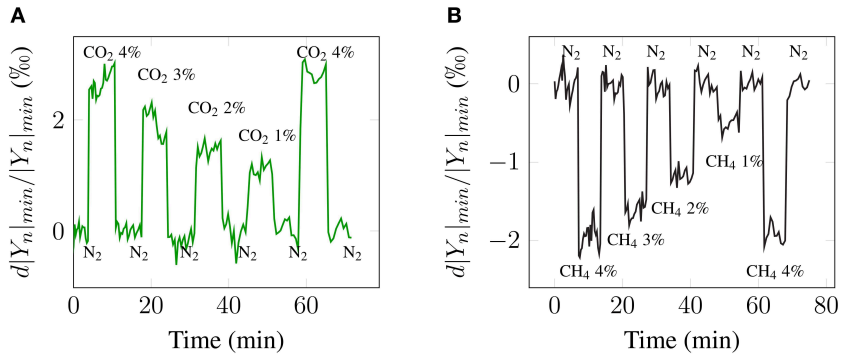

FIGURE 6 | Measurement for $V_{dc} = 35$V of $d|Y_n|_{min}/|Y_n|_{min}$ (drift removed) by alternating pure N_2 and either CO_2 **(A)** or CH_4 **(B)** in different concentrations (4%, 3%, 2%, 1%, and 4%).

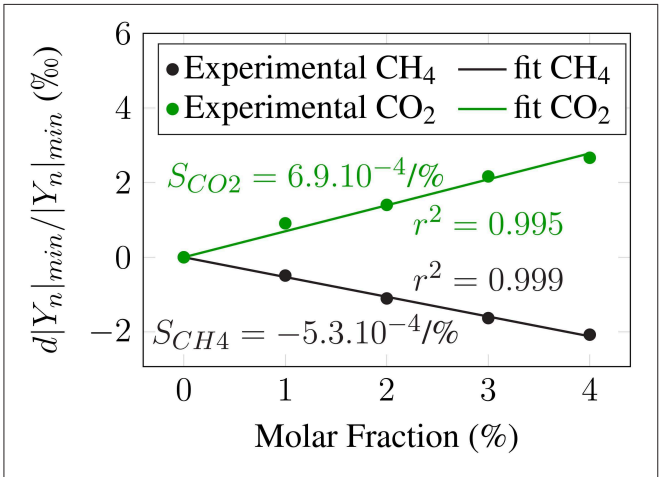

FIGURE 7 | Sensor output characteristic for CO_2 (green) and CH_4 (black).

TABLE 2 | Measured values of S for $V_{dc} = 35$V and reported values of $d\rho/\rho$ and $d\eta/\eta$ according to previous work (Iglesias et al., 2019).

Mixture	N_2-CO_2	N_2-CH_4
S (/%)	$6.9.10^{-4}$	$-5.3.10^{-4}$
$d\rho/\rho$ (%) at 1% in N_2 and 20°C 1atm	0.56	−0.42
$d\eta/\eta$ (%) at 1% in N_2 and 20°C 1atm	−0.20	−0.41

Q_a with values from **Table 2**, it can be shown that $|a/b| = 5.6$. This means that (assuming that Equation 36 holds for a square membrane) this sensing method would be more suitable to detect gases that would induce an important change in the gas mass density ρ rather than for gases that would only induce it in the gas viscosity η. That being said, the influence of the viscosity remains non-negligible.

3.2. Limit of Detection

Once the sensitivity measured, an estimation of the limit of detection (LOD) for each gas (CO_2 or CH_4) can be estimated (Equation 35). For this, the noise standard deviation of $d|Y_n|_{min}/|Y_n|_{min}$ ($\sigma = 0.11$‰) was measured under pure N_2. The computed values both for CO_2 and CH_4 (respectively $LOD_{CO2} = 0.5\%$ and $LOD_{CH4} = 0.6\%$) were then tested experimentally with an appropriate sequence of lower concentrations for each gas (1%, 0.75%, 0.5%, 0.25%, 1% for CO_2 and 1%, 0.8%, 0.6%, 0.4%, 1% for CH_4). The results are shown in **Figure 8** and are consistent with the calculations.

4. CONCLUSION

In conclusion, an analytical model of the influence of the bias voltage in the sensitivity when measuring the value of the normalized admittance at either the resonance or the anti-resonance of a CMUT was presented. This model showed that the sensitivities at both the resonance and anti-resonance are comparable although slightly higher at the anti-resonance. Experiments have been performed by measuring the admittance value at the anti-resonance which is much more sensitive for the tested device than measuring the resonant frequency which is more classical in the community of resonant gas sensors. The expression of the sensitivity at the anti-resonance was verified at different values of the bias voltage in the context of gas sensing without sensitive coating. Examples of measurements were presented for mixtures of N_2 and either CO_2 or CH_4 for which a sensitivity of $6.9.10^{-4}$% and $-5.3.10^{-4}$/% were

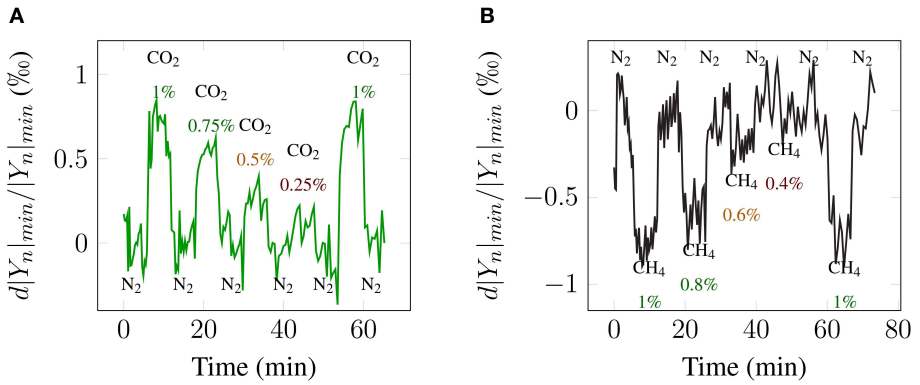

FIGURE 8 | Measurement for $V_{dc} = 35$V of $d|Y_n|_{min}/|Y_n|_{min}$ (drift removed) by alternating pure N_2 and either CO_2 at 1%, 0.75%, 0.5%, 0.25%, and 1% **(A)** or CH_4 at 1%, 0.8%, 0.6%, 0.4%, and 1% **(B)**. The concentrations were chosen in order to estimate their respective *LOD*.

obtained, respectively, and limits of detection of 0.5% and 0.6% were demonstrated, respectively. Such values could potentially be improved by further optimization of other parameters such as the geometry of the CMUT. Combining the presented measurements with other sensors could also compensate for the lack of selectivity to extend the capabilities beyond binary mixtures.

DATA AVAILABILITY STATEMENT

The datasets generated for this study are available on request to the corresponding author.

AUTHOR CONTRIBUTIONS

PS, J-FM, DA, and DC have designed and fabricated the CMUTs. LI and ID have developed the modeling and data treatments. LI has done the measurements. All the authors have contributed to the writing of the paper.

FUNDING

This research was performed thanks to the contest Programme d'Investissements d'Avenir of the French Goverment under the supervision of the French National Radioactive Waste Management Agency (ANDRA).

ACKNOWLEDGMENTS

The authors would like to thank Laurent Colin from GREMAN for the design of the PCB where the CMUTs chips were wired to and the fabrication of the cell allowing the gas to flow over the CMUTs.

REFERENCES

Abdolrazzaghi, M., and Daneshmand, M. (2016). "Enhanced Q double resonant active sensor for humidity and moisture effect elimination," in *2016 IEEE MTT-S International Microwave Symposium (IMS)* (San Francisco, CA: IEEE), 1–3.

Boudjiet, M., Cuisset, V., Pellet, C., Bertrand, J., and Dufour, I. (2014). Preliminary results of the feasibility of hydrogen detection by the use of uncoated silicon microcantilever-based sensors. *Int. J. Hyd. Energy* 39, 20497–20502. doi: 10.1016/j.ijhydene.2014.03.228

Daynes, H. A. (1933). Gas analysis by measurement of thermal conductivity. Cambridge University Press 1933. VIII + 357 S. m. 76 Abb. Preis 16/- sh. *Z. angew. Math. Mech.* 13, 328–328. doi: 10.1002/zamm.19330130419

Göpel, W. (1994). New materials and transducers for chemical sensors. *Sens. Actuat. B Chem.* 18, 1–21. doi: 10.1016/0925-4005(94)87049-7

Gurun, G., Hasler, P., and Degertekin, F. (2011). Front-end receiver electronics for high-frequency monolithic CMUT-on-CMOS imaging arrays. *IEEE Trans. Ultrason. Ferroelect. Freq. Contr.* 58, 1658–1668. doi: 10.1109/TUFFC.2011.1993

Hale, J., Stehle, G., and Bals, I. (1992). Gas analysis using a thermal conductivity method. *Sens. Actuat. B Chem.* 7, 665–671. doi: 10.1016/0925-4005(92)80383-9

Haller, M., and Khuri-Yakub, B. (1996). A surface micromachined electrostatic ultrasonic air transducer. *IEEE Trans. Ultrason. Ferroelectr. Freq. Cont.* 43, 1–6. doi: 10.1109/58.484456

Heinisch, M., Voglhuber-Brunnmaier, T., Reichel, E., Dufour, I., and Jakoby, B. (2015). Application of resonant steel tuning forks with circular and rectangular cross sections for precise mass density and viscosity measurements. *Sens. Actuat. A Phys.* 226, 163–174. doi: 10.1016/j.sna.2015.02.007

Heller, J., Boulme, A., Alquier, D., Ngo, S., and Certon, D. (2018). Performance evaluation of CMUT-based ultrasonic transformers for galvanic isolation. *IEEE Trans. Ultrason. Ferroelectr. Freq. Cont.* 65, 617–629. doi: 10.1109/TUFFC.2018.2796303

Iglesias, L., Boudjiet, M., and Dufour, I. (2019). Discrimination and concentration measurement of different binary gas mixtures with a simple resonator through viscosity and mass density measurements. *Sens. Actuat. B Chem.* 285, 487–494. doi: 10.1016/j.snb.2019.01.070

Korotcenkov, G., and Cho, B. (2011). Instability of metal oxide-based conductometric gas sensors and approaches to stability improvement (short survey). *Sens. Actuat. B Chem.* 156, 527–538. doi: 10.1016/j.snb.2011.02.024

Koymen, H., Atalar, A., and Tasdelen, A. S. (2017). Bilateral CMUT cells and arrays: equivalent circuits, diffraction constants, and substrate impedance. *IEEE Trans. Ultrason. Ferroelect. Freq. Contr.* 64, 414–423. doi: 10.1109/TUFFC.2016.2628882

Lange, D., Hagleitner, C., Hierlemann, A., Brand, O., and Baltes, H. (2002). Complementary metal oxide semiconductor cantilever arrays on a single chip: mass-sensitive detection of volatile organic compounds. *Anal. Chem.* 74, 3084–3095. doi: 10.1021/ac011269j

Lee, H. J., Park, K. K., Cristman, P., Oralkan, O., Kupnik, M., and Khuri-Yakub, B. T. (2009). "A low-noise oscillator based on a multi-membrane CMUT for high sensitivity resonant chemical sensors," in *2009 IEEE 22nd International Conference on Micro Electro Mechanical Systems* (Sorrento: IEEE), 761–764. doi: 10.1109/MEMSYS.2009.4805494

Lee, H. J., Park, K. K., Kupnik, M., Oralkan, O., and Khuri-Yakub, B. T. (2011). Chemical vapor detection using a capacitive micromachined ultrasonic transducer. *Anal. Chem.* 83, 9314–9320. doi: 10.1021/ac201626b

Park, K. K., Lee, H. J., Yaralioglu, G. G., Ergun, A. S., Oralkan, O., Kupnik, M., et al. (2007). Capacitive micromachined ultrasonic transducers for chemical detection in nitrogen. *Appl. Phys. Lett.* 91:094102. doi: 10.1063/1.2776348

Qiu, Y., Gigliotti, J. V., Wallace, M., Griggio, F., Demore, C. E., Cochran, S., et al. (2015). Piezoelectric micromachined ultrasound transducer (PMUT) arrays for integrated sensing, actuation and imaging. *Sensors* 15, 8020–8041. doi: 10.3390/s150408020

Romain, A., and Nicolas, J. (2010). Long term stability of metal oxide-based gas sensors for e-nose environmental applications: an overview. *Sens. Actuat. B Chem.* 146, 502–506. doi: 10.1016/j.snb.2009.12.027

Rosario, R., and Mutharasan, R. (2014). Piezoelectric excited millimeter sized cantilever sensors for measuring gas density changes. *Sens. Actuat. B Chem.* 192, 99–104. doi: 10.1016/j.snb.2013.10.017

Sader, J. E. (1998). Frequency response of cantilever beams immersed in viscous fluids with applications to the atomic force microscope. *J. Appl. Phys.* 84, 64–76. doi: 10.1063/1.368002

Shanmugam, P., Iglesias, L., Michaud, J. F., Dufour, I., Alquier, D., Colin, L., et al. (2018). "CMUT based air coupled transducers for gas-mixture analysis," in *2018 IEEE International Ultrasonics Symposium (IUS)* (Kobe), 1–4.

Sharma, R. K., Chan, P. C., Tang, Z., Yan, G., Hsing, I.-M., and Sin, J. K. (2001). Investigation of stability and reliability of tin oxide thin-film for integrated micro-machined gas sensor devices. *Sens. Actuat. B Chem.* 81, 9–16. doi: 10.1016/S0925-4005(01)00920-0

Simon, I., and Arndt, M. (2002). Thermal and gas-sensing properties of a micromachined thermal conductivity sensor for the detection of hydrogen in automotive applications. *Sens. Actuat. A Phys.* 97–98, 104–108. doi: 10.1016/S0924-4247(01)00825-1

Tétin, S., Caillard, B., Ménil, F., Debéda, H., Lucat, C., Pellet, C., et al. (2010). Modeling and performance of uncoated microcantilever-based chemical sensors. *Sens. Actuat. B Chem.* 143, 555–560. doi: 10.1016/j.snb.2009.09.062

Toda, H., and Kobayakawa, T. (2008). High-speed gas concentration measurement using ultrasound. *Sens. Actuat. A Phys.* 144, 1–6. doi: 10.1016/j.sna.2007.12.025

Törndahl, M., Almqvist, M., Wallman, L., Persson, H., and Lindstrom, K. (2002). "Characterisation and comparison of a cMUT versus a piezoelectric transducer for air applications," in *2002 IEEE Ultrasonics Symposium, 2002. Proceedings*, Vol. 2 (Munich: IEEE), 1023–1026.

Um, J.-Y., Kim, Y.-J., Cho, S.-E., Chae, M.-K., Song, J., Kim, B., et al. (2014). An analog-digital hybrid RX beamformer chip with non-uniform sampling for ultrasound medical imaging with 2d CMUT array. *IEEE Trans. Biomed. Circuits Syst.* 8, 799–809. doi: 10.1109/TBCAS.2014.2375958

Wenchao, Z., Ting, Y., and Fengqi, Y. (2008). "A 1-D lumped theoretical model for CMUT," in *2008 IEEE/ASME International Conference on Advanced Intelligent Mechatronics* (Xian: IEEE), 318–322. doi: 10.1109/AIM.2008.4601680

Wygant, I. O., Kupnik, M., and Khuri-Yakub, B. T. (2016). "CMUT design equations for optimizing noise figure and source pressure," in *2016 IEEE International Ultrasonics Symposium (IUS)* (Tours: IEEE), 1–4.

Wygant, I. O., Zhuang, X., Yeh, D. T., Oralkan, O., Sanli Ergun, A., Karaman, M., et al. (2008). Integration of 2d CMUT arrays with front-end electronics for volumetric ultrasound imaging. *IEEE Trans. Ultrason. Ferroelect. Freq. Contr.* 55, 327–342. doi: 10.1109/TUFFC.2008.652

Yaralioglu, G. G., Ergun, A. S, Bayram, B., Haeggström, E., and Khuri-Yakub, B. T. (2003). Calculation and measurement of electromechanical coupling coefficient of capacitive micromachined ultrasonic transducers. *IEEE Trans. Ultrason. Ferroelect. Freq. Contr.* 50, 449–456. doi: 10.1109/tuffc.2003.1197968

Conflict of Interest: The authors declare that the research was conducted in the absence of any commercial or financial relationships that could be construed as a potential conflict of interest.